Sheffield Hallam University

Numerical Inspection based on Quasi-Static Analysis using Rousselier Damage Model for Aluminium Wingbox Aircraft Structure.

AHMAD, MIM, CURIEL-SOSA, JL, AKBAR, Mahesa and ABDULLAH, NA

Published version

PAPER • OPEN ACCESS

Numerical Inspection based on Quasi-Static Analysis using Rousselier Damage Model for Aluminium Wingbox Aircraft Structure

View the article online for updates and enhancements.

IOP ebooks™

Bringing you innovative digital publishing with leading voices to create your essential collection of books in STEM research.

Start exploring the collection - download the first chapter of every title for free.

Numerical Inspection based on Quasi-Static Analysis using Rousselier Damage Model for Aluminium Wingbox Aircraft Structure

M.I.M. Ahmad[1,2], J.L. Curiel-Sosa[1], M. Akbar[1], N.A. Abdullah[1]

[1]Computer-Aided Aerospace and Mechanical Engineering Research Group (CA[2]M), The University of Sheffield, Sheffield, UK

[2]Department of Mechanical and Materials Engineering, Faculty of Engineering and Build Environments, University Kebangsaan Malaysia, 43600 UKM Bangi, Selangor, Malaysia

E-mail: `mimeorahmad1@sheffield.ac.uk`

Abstract. The present paper illustrates a modelling technique of void damage prediction using constitutive Rousselier damage model in wingbox aircraft structure. The high possibility of aluminium wingbox structure to deform during operating become a driving force in this study. The Rousselier model is implemented by the user-defined material subroutine UMAT in the ABAQUS/ Standard. The wingbox is a part of a commercially-made commuter aircraft prototype, in which steady aerodynamic pressure is applied as the quasi-static, ranging from cruise load factor until the ultimate load factor. This analysis is divided into three assessments: load factor assessment, damage detection and implementation of Rousselier-UMAT-XFEM (RuX) model solution. The results indicate the maximum stress concentration occurs at the bottom-root part of the skin. The void volume fraction and the crack grow as the load factor increases to the ultimate load factor. A comparison with the literature is shown in some details.

1. Introduction

Aircraft structural members are designed to carry a load and resist the stress during operation. The significant effect on the aerodynamic performance of the aircraft existed due to material deform during the extreme condition on the flight. Several studies have been done to investigate the behaviour of damage occur in the aircraft structure in order to improve and to make sure it is safe during flight. In experimental approach, Sundaresan et al. 2003 [1] discussed the damage detection on a wing panel inside the wingbox using vibration detection shapes. Following with mathematical investigation by Grondel et al. 2004 [2], which has developed a health monitoring system to detect the damaging impact of the wingbox structure. Then, Chen et al. 2007 [3] proposed a dynamic-based damage detection method in composite wingbox structure using Hillbert-Huang transform (HHT).

Another method that can be applied is by using continuum damage mechanics (CDM) model [4, 5]. Previously, the CDM model based on Hashin failure criterion was used to model the damage assessment of rotary wing aircraft cabin door [6]. In this study, the numerical inspection based on Rousselier damage criteria of CDM model is investigated in wingbox structure where most of the wings's load is carried [7]. The Rousselier model, which has been introduced over last two decades, has become a powerful tool for modelling the damage criteria in structural analysis.

For example of the model application such as in predicting the fracture resistant behaviour of Zircaloy fuel pin specimens [8], simulation damage behaviour in eletron beam welded joints [9] and welded Esshete 1250 pipe [10]. This model can predict the behaviour of materials from the micromechanics processes leading to ductile fracture [11, 12]. From the authors' knowledge, this is a first attempt that the structural analysis is proposed for an aircraft wingbox by using the Rousselier damage model, in order to represent the damage behaviour of the material. Moreover, further investigation is carried out by implementing the Rousselier model with the XFEM solution, so called RuX model, to predict the void damage with the crack development in the material.

2. Numerical frameworks

2.1. Rousselier's Damage Model

Rousselier damage model was implemented using an Abaqus UMAT subroutine to describe the material damage. In the subroutine, the integration scheme utilizing the radial return algorithm and implicit solution method are formulated in the finite element method. The Rousselier plastic potential is used to estimate the onset of yielding of the material point which shows the presence of the void volume fraction, considered as an internal state variable in the material constitutive model. Rousselier[13] proposed the classical plastic potential as:

$$\phi = \frac{q}{\rho} - R\left(\varepsilon_{eq}\right) + B\left(\beta\right) D e^{\left(\frac{-p}{\rho\sigma_1}\right)} \tag{1}$$

where q and p are the von Mises equivalent stress and hydrostatic pressure respectively, D and σ_1 are Rousselier material parameters, ρ is a relative density, β is an internal variable describing damage and ε_{eq} is the equivalent plastic strain which represents hardening of the material. With loading, the void volume fraction evolves from the initial void volume fraction, f_0, of the material. The void growth rate can be obtained as:

$$\dot{f} = (1 - f)\dot{\epsilon}^p_{kk} = (1 - f)\dot{\epsilon}_p \tag{2}$$

where $\dot{\varepsilon}^p_{kk}$ is the component of the plastic strain tensor.

By considering a material which contains a void, the relationship between the relative density, ρ, and f can be written as:

$$\rho = \left(\frac{1 - f}{1 - f_0}\right) \tag{3}$$

since the value of f_0 is very small compared to unity, Eq. (3) becomes as [14]:

$$\rho = 1 - f \tag{4}$$

However, f_0 is still be calculated in the formulation of this study, in order to see the influence of f_0 in the formation of void growth in the material. The function of $B\left(\beta\right)$ in Eq. (1) can be written in terms of the void volume fraction as:

$$B\left(\beta\right) = \sigma_1 f \tag{5}$$

By substituting Eq. (4) and Eq. (5) into Eq. (1), the Rousselier plastic potential can be written as:

$$\phi = \frac{q}{1 - f} - R\left(\varepsilon_{eq}\right) + D\sigma_1 f e^{\left(\frac{-p}{(1-f)\sigma_1}\right)} \tag{6}$$

To establish the yield criterion, the values of yield function, ϕ are classified as follow:

$$\phi \leq 0 : \text{Elastic deformation regime} \tag{7}$$

$$\phi > 0 : \text{Plastic deformation regime} \tag{8}$$

3. Technical wingbox structure

The layout of the wingbox used in the present work is shown in Fig. 1. The wingbox prototype is developed under the joint program of Indonesian Aerospace, National Institute of Aeronautics and Space of Indonesia and Agency for Assessment and Application of Technology of Indonesia. Fig. 2 shows a wingbox structure which consists of spars, ribs, stringers and skin.
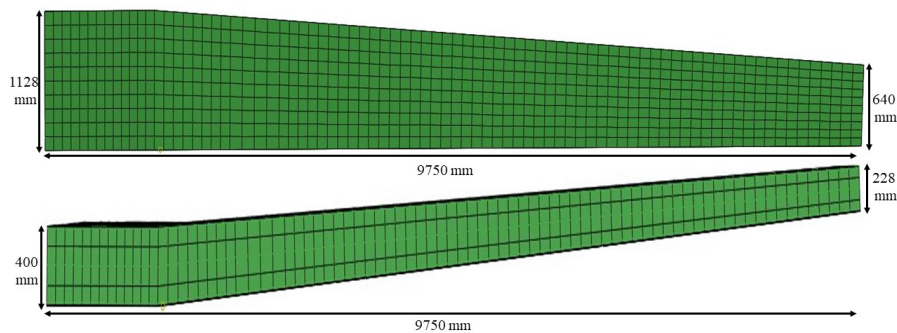
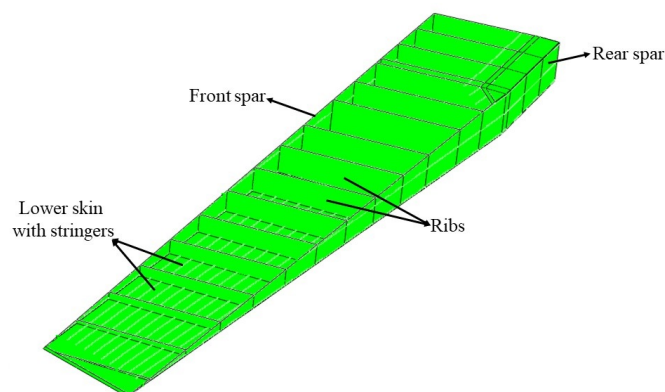**Figure 1.** Wingbox layout (top and side view)

Figure 2. Wingbox structure

The wingbox model consists of three type of elements, which are B31: 2-node linear beam, S4R: 4 node thick shell with reduced integration and hourglass control and C3D81: 8-node linear brick with the incompatible mode. For the boundary condition, the quasi-static load obtained from aerodynamic analysis is applied and fixed support in all-direction at the root of the wing, as shown in Fig. 3. The load increment is considered in terms of load factor, N. Initially no load condition is increased until the appropriate cruise load condition (N=1). It is further increased until ultimate load condition, which is 2.5 times cruise load (N=2.5). The details mechanical properties of the wingbox materials and hardening data can be accessed in Table 1 and 2, respectively.
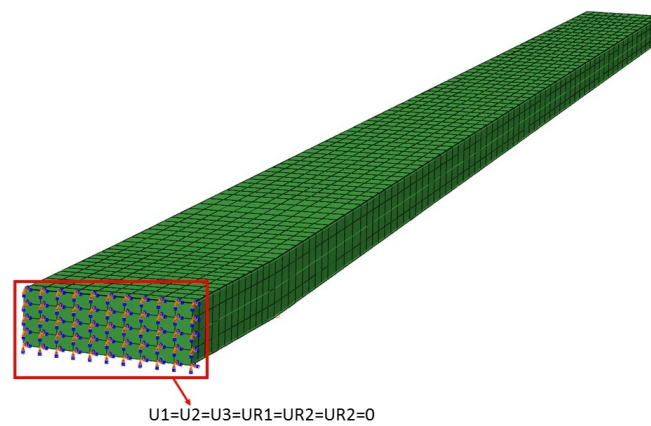

U1=U2=U3=UR1=UR2=0

Figure 3. Boundary conditions applied to the wingbox structure

Table 1. Mechanical properties and Rousselier parameters of 6065-T6, aluminium alloy [15]

Young modulus, GPa, (E)	68.9
Poisson ratio, (v)	0.33
Yield strength, MPa, (σ_y)	270
Rousselier parameter, MPa, (σ_1)	180
Rousselier parameter, (D)	2
Initial void volume fraction, (f_o)	0.0001

Table 2. Hardening data [16]

True strain, (ϵ_T)	True stress, MPa, (σ_T)
0.012	296
0.0182	301
0.027	309
0.0396	320
0.0509	330
0.0641	338
0.079	348
0.0926	355
0.1028	359
0.1129	361

4. Load factor assessment

As explained in Section 3, aerodynamic pressure is applied as the quasi-static load. The steady aerodynamic pressure is calculated using Lifting-Line Theory (LLT)[17, 18]. The LLT provides an analytical treatment for the evaluation of the aerodynamics of a finite wing, which is in the form of an infinite sine series for the circulation distribution, as shown in Fig. 4.
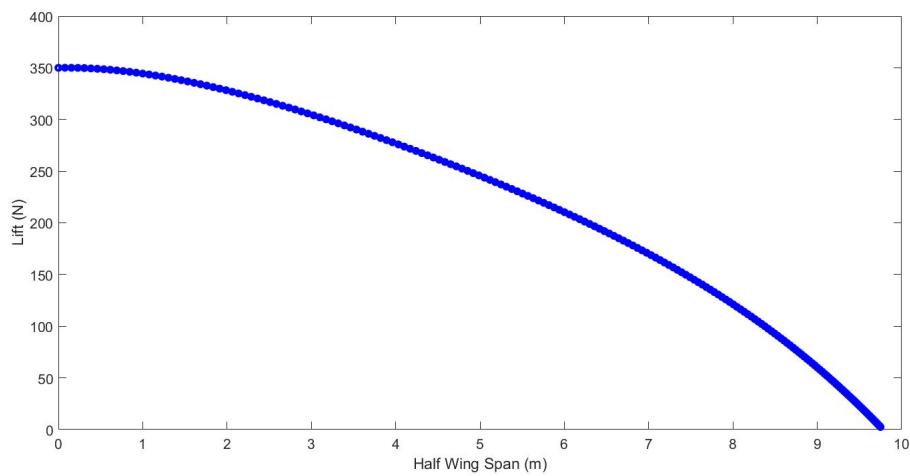
Figure 4. Aerodynamics lift distribution

Figs. 5 and 6 present the distribution of stresses at the top and bottom skin of the wingbox, where it can be seen that the maximum stresses concentration occurs in the region near the root section. As expected, the highest load factor influenced the formation of highest stress in the wingbox structure, which create 139 MPa in N=1, 208 MPa in N=1.5 and 305 MPa in N=2.5. Then, the distribution of the maximum principal strain along the wingbox structure is shown in Fig. 7. From Figs. 5, 6 and 7 (a and b), the contour plots do not show any significant difference in their patterns distribution due to deformation within elastic region during a load increment. Meanwhile, the wingbox structure deformed plastically during the ultimate load condition, where the void damage starts to grow. The formation of the void volume fraction along the wingbox structure can be seen as shown in Fig. 8.
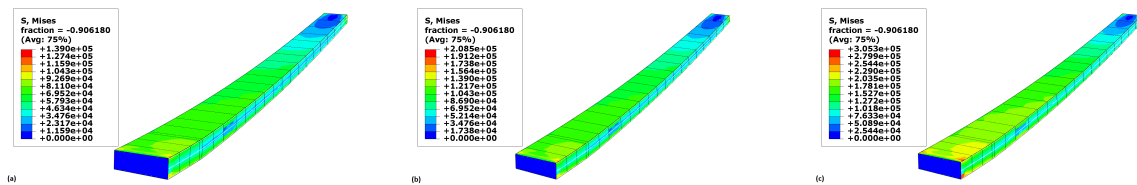

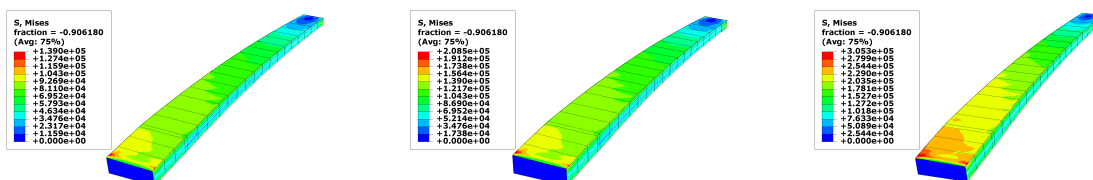**Figure 5.** Von Mises stress at a)N=1, b)N=1.5 and c)N=2.5 along the upper skin of wingbox structure

Figure 6. Von Mises stress at a)N=1, b)N=1.5 and c)N=2.5 along the bottom skin of wingbox structure
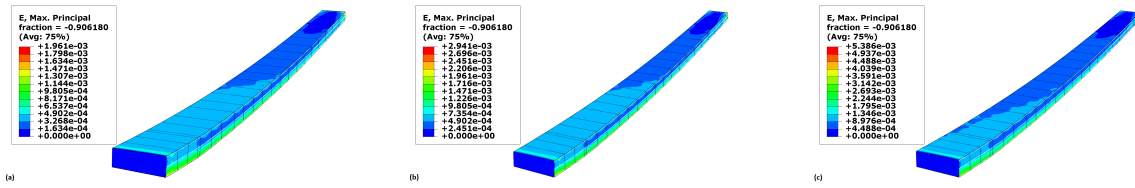
Figure 7. Maximum principal strain at a)N=1, b)N=1.5 and c)N=2.5 along the upper skin wingbox structure
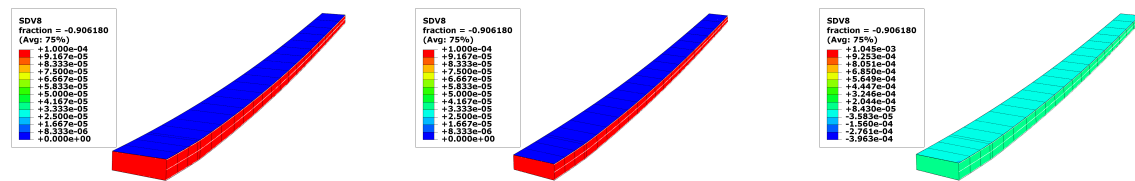

Figure 8. Void volume fraction at a)N=1, b)N=1.5 and c)N=2.5 along the upper skin wingbox structure

As can be seen clearly in Fig. 8(a and b), the contour plots also do not show any significant different, and the values of void damage are still below the value of the initial void volume fraction ($f_o = 0.0001$). However, the void damage emerged during the ultimate load condition as shown in Fig. 8(c), which represents the values of the void damage distribution along the wingbox structure. To determine the maximum displacement acting in the wingbox structure, Fig. 9 is depicted, which bring the maximum displacement of 724 mm in N=2.5, followed by 434 mm in N=1.5 and 289 mm in N=1. Therefore, it means that the wingbox structure design is safe from damage under the consideration of load factor range from 1-1.5. However, its need more attention concerning the safety of the wingbox structure with a situation of load factor in 2.5 or above.
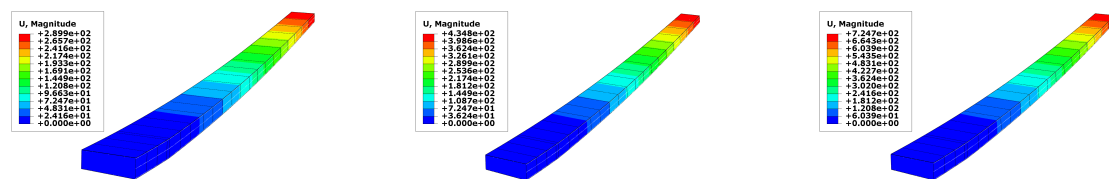

Figure 9. Displacement at a)N=1, b)N=1.5 and c)N=2.5 along the upper skin wingbox structure

Next, the comparison of stress-strain relation with the literature's result [19] is shown in Fig. 10. The benchmark results are considered under static load analysis, thus provides the stress-strain point for every increment of load factor. As a result, it shows that a good comparison has been achieved between both results in the load factor of 1 and 1.5 respectively. This finding can be verified by calculating the numerical value of similarity where it has revealed that 84%-86% similarity between a predicted value and benchmark value. Nevertheless, the comparison of stress-strain in the ultimate load factor gives small variances different, which admit 75% similarity. This is due to of different finite element formulation that used to represent the plasticity behaviour of the wingbox structure. In overall, the trend shows a reasonable agreement between both results and the validity of the result is successfully verified.
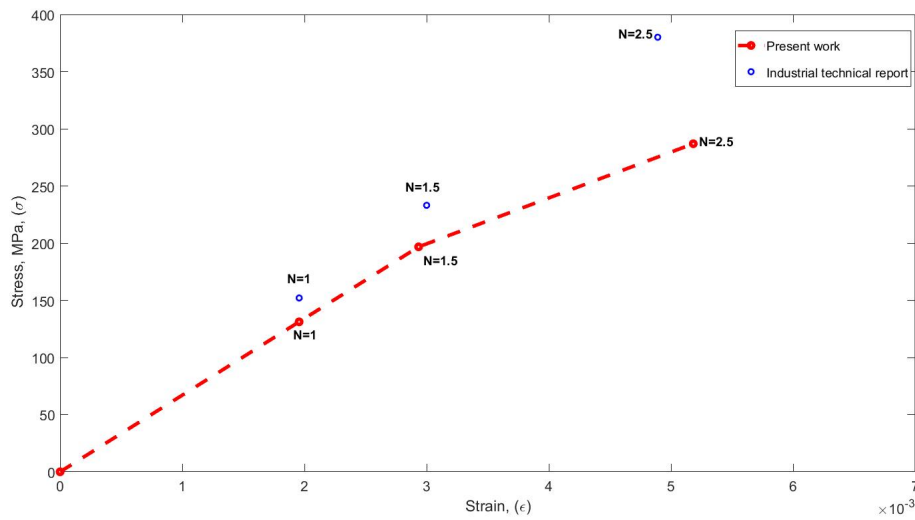
Figure 10. Stress strain relation with different load factors

5. Damage detection

This assessment is focused on the ultimate load factor, where the formation of void damage exists in the wingbox structure. The relationship between the void volume fraction and the strain is plotted as shown in Fig. 11. The initial void volume fraction, f_o, is increased with the increase of the strain, which revealed that the strain distribution had influenced the formation of the void damage, thus affect the material behaviour of wingbox structure to deform plastically.
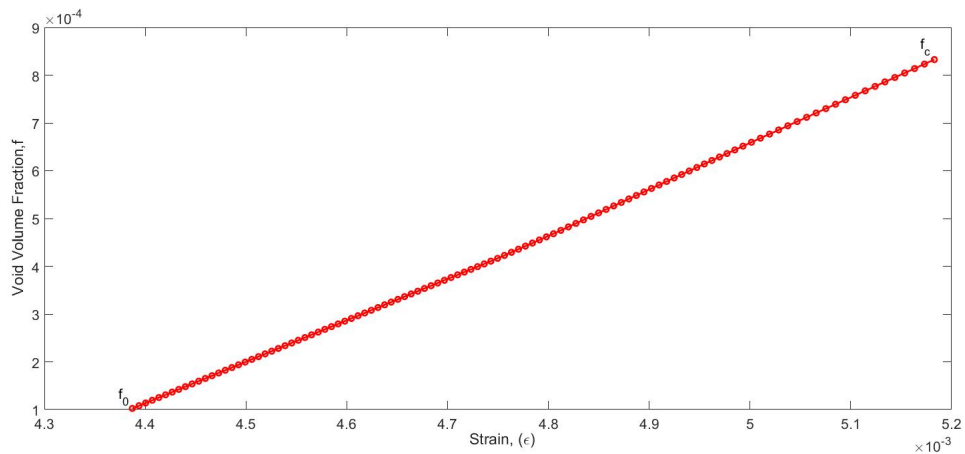

Figure 11. Void volume fraction with strain relation

To justify the results of damage model used in this analysis, the contour damage has been compared with the results from technical report [19]. Fig. 12 shows a damage parameter based on the failure indices criteria which is stated as more than one. In that case, the wingbox structure is suffering from fully damaged at the bottom skin of the root wing under the ultimate load condition. While from Fig. 13, the void damage based on the void volume fraction parameter is detected forms at the same location with the damaged region from the benchmark result and

the value of critical void volume fraction, f_c is recorded approximately as 0.001. Thus, a good reasonable comparison has been achieved and verified.
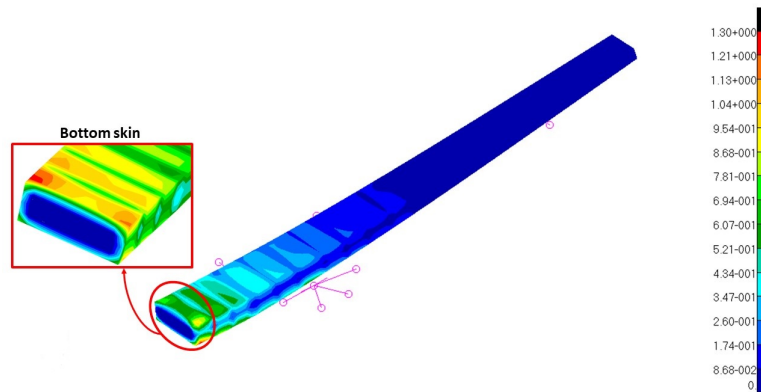

Figure 12. Failure indices in wingbox structure issued by industrial technical report [19] based on Hill theory
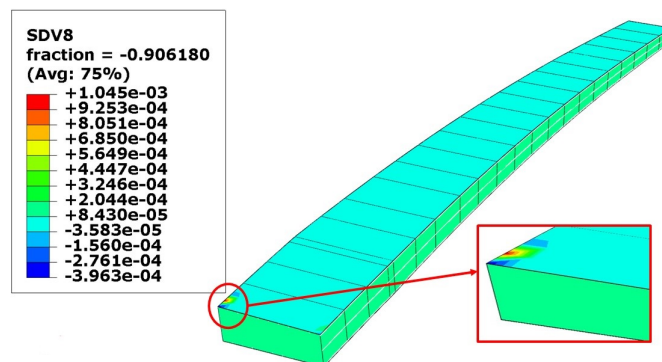

Figure 13. Void damage in wingbox structure based on the Rousselier damage model

6. Implementation of RuX model

RuX model solution has been proposed to predict the micromechanical damage of the material with the existing of the crack development. The RuX model is a combined term of the Rousselier model (constitutive damage model), UMAT subroutine (interface user-defined material) and XFEM solution (crack development). Fig. 14 illustrates the flow-diagram, displaying the steps involved in the model.

The XFEM provides a significant benefits in the numerical modelling of crack propagation where a discontinuous function is added to the finite element approximation of the displacement field [20, 21, 22, 23]. This solution is proposed where the crack initiation and evolution based on the damage of traction-separation law and displacement/ energy release rate criterion are selected for characterizing the crack behaviour, as shown in Table 3. Fig. 15 shows how the crack is propagated due to the void growth detected at the bottom skin of the root of the wingbox structure. As expected, the crack was initiated, and then it has propagated in the region
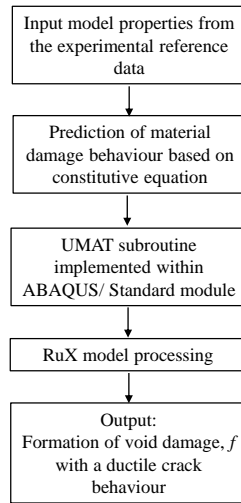
Figure 14. The flow diagram of RuX model

where the concentration of maximum stresses existed. It gives a good sign for RuX model as a constitutive damage model to predict the void-crack damage of the material behaviour problem.

Table 3. Material parameter and fracture toughness values of 6065-T6, aluminium alloy [24]

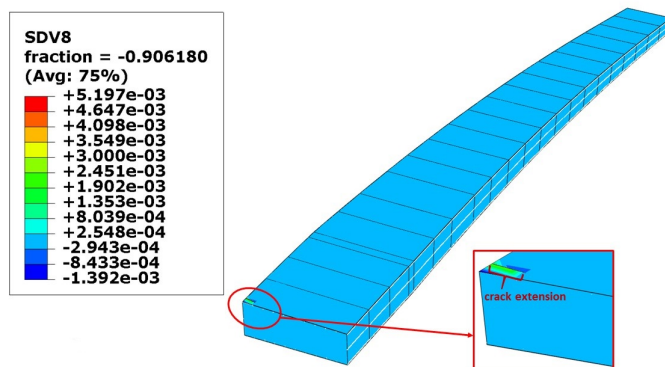|	
Max principal stress, MPa	310
Fracture energy, kJ/m^2, (G_{Ic})	121

Figure 15. Formation of void damage and crack propagation at the root-bottom skin of the wingbox structure

6.1. Relative error

The evaluation of relative error is conducted to validate the stability and accuracy of the simulation results. In this case, the residual displays information determines either an iteration has produced an equilibrium solution [25]. It can be seen in Fig. 16, a solution achieved a stable condition and the data recorded are below the tolerance value, which sets to 0.005.
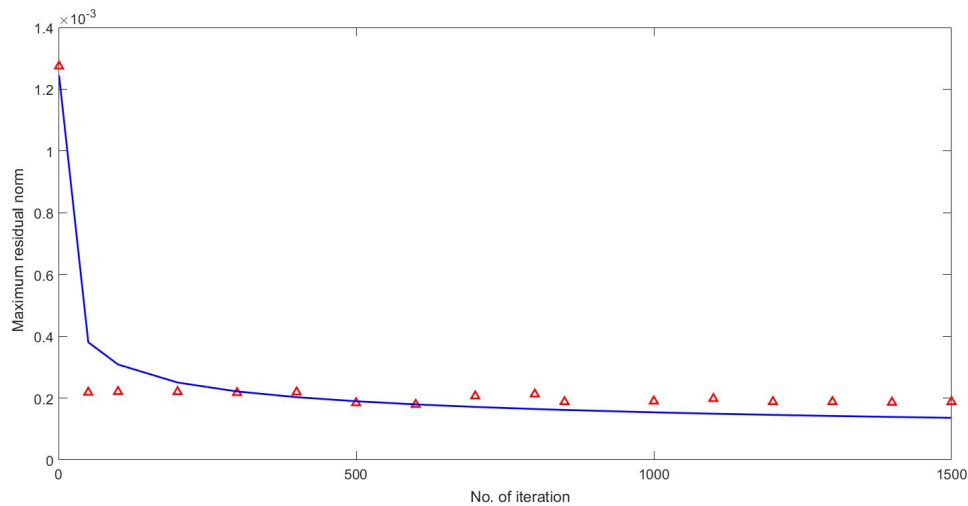

Figure 16. Maximum residual norm vs No. of iteration

7. Conclusion

This research has presented a structural analysis of aluminium wingbox aircraft structure based on quasi-static analysis using constitutive Rousselier damage model. The ability of this model to define the material damage behaviour of the wingbox structure become a novel achievement of this research finding. The investigation with the proposed numerical solution resulted in the following:

- The Rousselier damage model was successfully installed in the user-defined material subroutine UMAT in the ABAQUS/ Standard.
- The aerodynamic distributed forces were calculated using the Lifting-Line Theory (LLT). By referring to the indicator of load factor, N, the highest stresses created: 139 MPa in N=1, 208 MPa in N=1.5 and 305 MPa in N=2.5. It is well predicted when the results have been compared from previous literature and show a good agreement between both results.
- The damage was formed at the bottom skin of the root wing, and it is verified by comparing the result from previous literature. The results show a good agreement have been achieved between both results.
- The crack development has been introduced by the RuX model solution, which purposes to predict the void damage and the position of the crack in the wingbox structure. As been expected, the crack was initiated and extended in the area of the formation of the void damage, where the maximum stress concentrates at the same place.

8. Acknowledgments

References

[1] Sundaresan M.J, Ghoshal A, Li J, Schulz M.J, Pai P.F and Chung J.H. Experimental damage detection on a wing panel using vibration deflection shapes, Structural Health Monitoring. 2003, 2(3): 243-256.
[2] Grondel S, Assad J, Delebarre C and Moulin E. Health monitoring of a composite wingbox structure, Ultrasonics. 2004, 42(1-9): 819-824.
[3] Chen H.G, Yan Y.J and Jiang J.S. Vibration-based damage detection in composite wingbox structures by HHT, Mechanical Systems and Signal Processing. 2007, 21(1): 307-321.
[4] Chaboche J.L, Boudifa M and Saanouni K. A CDM approach of ductile damage with plastic compressibility, International Journal of Fracture. 2006, 137: 51-75.
[5] Besson J. Continuum models of ductile fracture: a review, International Journal of Damage Mechanics. 2010, 19: 1-52.
[6] Gangadhara Rao T.B, Vijaya K.R and Subba R.V.V. Numerical modelling and damage assessment of rotary wing aircraft cabin door using continuum damage mechanics model, Applied Composite Materials. 2017, 24(1): 235-250.
[7] Akbar M and Curiel-Sosa J.L. Piezoelectric energy harvester composite under dynamic bending with implementation to aircraft wingbox structure, Composite Structures. 2016, 153: 193-203.
[8] Samal M.K and Shah P.K. On the application of Rousselier's damage model to predict fracture resistance behavior of zircaloy fuel pin specimens, Procedia Engineering. 2013, 55: 710-715.
[9] Tu H.Y, Schmauder S, Weber U, Rudnik Y and Ploshikhin. Simulation of the damage behaviour of electron beam welded joints with the Rousselier model, Engineering Fracture Mechanics. 2013, 103: 153-161.
[10] Arun S, Sherry A.H, Smith M.C and Sheikh M. Simulations of the large-scale four point bending test using Rousselier model, Engineering Fracture Mechanics. 2017, 178: 497-511.
[11] Rousselier G, Devaux J-C, Mottet G and Devesa G. A methodology for ductile fracture analysis based on damage mechanics: An illustration of a local approach of fracture. STP27716S Nonlinear Fracture Mechanics: Volume II Elastic-Plastic Fracture, ASTM International, West Conshohocken, PA. 1988, 332-354.
[12] Rousselier G. Dissipation in porous metal plasticity and ductile fracture, Journal of The Mechanics and Physics of Solids. 2011, 49: 1727-1746.
[13] Rousselier G. Finite deformation constitutive relations including ductile fracture damage. Three-dimensional constitutive relations and ductile fracture, Amsterdam, North-Holland Publishing Co. 1981, 331-355.
[14] Rousselier G. Ductile fracture models and their potential in local approach of fracture, Nuclear Engineering and Design. 1987, 105(1): 97-111.
[15] Guo J, Zhao S, Murakami R and Zang S. Experimental and numerical investigation for ductile fracture of Al-alloy 5052 using modified Rousselier model, Computational Materials Science. 2013, 71: 115-123.
[16] Xu F, Zhang H, Zhao S, Chen C, Cao M and Chen W. Optimized calibration procedure of the damage parameters of 6082-T6 sheet, Materials. 2018, 11(2): 248.
[17] Pakalnis E. Lift and drag force calculation methods using non-linear section data. History and recent research, Aviation. 2010, 8:2, 9-13.
[18] Phillips W.F and Snyder D.O. Modern adaptation of Prandtl's classic Lifting-Line Theory, Journal of Aircraft. 2000, 37:4, 662-670.
[19] Scaling and Analysis of N219 Half Wing for Wind Tunnel Flutter Model Design, Structure Analysis Department, The Indonesian Aerospace (IAe) Company. Private and confidential.
[20] Belytschko T, Liu W, Moran B and Elkhodary K. Nonlinear finite elements for continua and structures, 2nd Ed. Wiley. 2013.
[21] Giner E, Sukumar N, Tarancn J and Fuenmayor F. An abaqus implementation of the extended finite element method, Engineering Fracture Mechanics. 2009, 76(3): 347-368.
[22] Curiel-Sosa J.L and Karapurath N. Delamination modelling of GLARE using the extended finite element method, Composite Science and Technology, 2012, 72: 788-791.
[23] Curiel-Sosa J.L, Tafazzolimoghaddam B and Zhang C. Modelling fracture and delamination in composite laminates: Energy release rate and interface stress, Composite Structures. 2018, 189: 641-647.

[24] P.S, Singh K.K, Tripathi V.K, Sarkar P.K and Kumar P. Fracture toughness of thin aluminium sheets using modified single edge notch specimen, International Journal of Engineering and Innovative Technology (IJEIT). 2012, 1(5): 283-288.

[25] Curiel-Sosa J.L, Beg O.A and Murillo J.M.L. Finite element analysis of structural instability using an implicit/ explicit switching technique, International Journal for Computational Methods in Engineering Science and Mechanics. 2013, 14(5): 452-264.